13

Optical-Thermal Phenomena in Polycrystalline Silicon MEMS During Laser Irradiation

Justin R. Serrano and Leslie M. Phinney
Engineering Sciences Center, Sandia National Laboratories
Albuquerque, New Mexico,
USA

1. Introduction

Many microelectromechanical systems (MEMS) applications utilize laser irradiation as an integral part of the system functionality, including projection displays, optical switches, adaptive optics (Andrews et al., 2011; Andrews et al., 2008), optical cross-connects (Knoernschild et al., 2009), and laser powered thermal actuators (Serrano & Phinney, 2008; Serrano et al., 2005). When laser irradiation is incident on small-scale systems, such as these MEMS applications, the propensity for exceeding the thermal handling capability of the devices dramatically increases, often leading to overheating, and subsequent deformation and permanent damage to the devices. In most instances, this damage is a direct consequence of the device geometry and the material thermal properties, which hinder the transport of heat out of any locally heated area. Such thermally-driven failures are common in electrically-powered systems (Baker et al., 2004; Plass et al., 2004). However, for laser-irradiated MEMS, particularly those fabricated of surface-micromachined polycrystalline silicon (polysilicon), the optical properties can also affect the thermal response of the devices by altering how the laser energy is deposited within the material. Even more concerning in these types of devices is the fact that the thermal, optical, and mechanical response can be intimately coupled such that predicting device performance becomes difficult. In this chapter, we focus on understanding some of the basics of optical interactions in laser-irradiated MEMS. We will first look at how the optical properties of the materials affect the laser energy deposition within a device. We will then expand upon this by looking at the coupling that exists between the optical and thermal properties, paying particular attention to the implications that transient temperature changes have in the optical response, ultimately leading to device failure. Finally, we will look at various cases of laser-induced damage in polysilicon MEMS where the device geometry and design and optical-thermal coupling have led to device failure.

2. Optical interactions in MEMS

Understanding the coupling that exists between the thermal and optical behavior in laser-irradiated MEMS must begin by looking at the optical properties of the irradiated materials and at how the laser light interacts with each material. The primary factor that affects the magnitude of this interaction is the material's complex refractive index, $\hat{n} = n + ik$. A wave

incident on the interface between two media of different refractive indices will undergo reflection and refraction, as shown in Fig. 1. The direction of the reflected and refracted beams follow the well-known laws of reflection and refraction:

$$\theta_r = \theta_i \text{ (law of reflection)}, \tag{1}$$

$$\hat{n}_2 \sin\theta_t = \hat{n}_1 \sin\theta_i \text{ (law of refraction; Snell's law)} \tag{2}$$

where θ_i, θ_r and θ_t are the angles of incidence, reflection, and refraction, respectively[1]. The following sections will discuss how the rules above are applied to laser-irradiated structures in order to obtain the magnitudes of the reflected, transmitted, and absorbed light, which ultimately dictate how the energy is deposited in an irradiated microsystem.

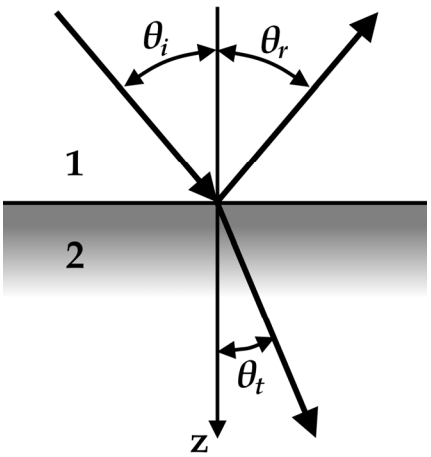

Fig. 1. Reflection and refraction of a plane wave incident on the interface between two media.

2.1 Optically thick systems

For monochromatic laser light, incident from vacuum ($\hat{n}_{vacuum} = 1.0$) at an angle θ_i upon a homogeneous, semi-infinite, non-magnetic medium of index $\hat{n}$, the reflectivity of the interface is dictated by the Fresnel coefficients (Born & Wolf, 1999):

$$r^s = \frac{\cos\theta_i - \sqrt{\hat{n}^2 - \sin^2\theta_i}}{\cos\theta_i + \sqrt{\hat{n}^2 - \sin^2\theta_i}}, \; r^p = \frac{\hat{n}^2\cos\theta_i - \sqrt{\hat{n}^2 - \sin^2\theta_i}}{\hat{n}^2\cos\theta_i + \sqrt{\hat{n}^2 - \sin^2\theta_i}}, \tag{3}$$

where the law of refraction was used to rewrite the expressions in terms of the incident angle and medium refractive index only, and the subscripts *s* and *p* above refer to the *s-polarized* or *transverse-electric* (TE) and *p-polarized* or *transverse-magnetic* (TM) polarizations of

[1] For instances where the indices are complex, the quantity θ_t is also complex-valued and no longer has the same meaning as an angle of refraction.

the incident light, respectively. The surface reflectivity, that is the magnitude of the fraction of reflected energy, is given for either polarization[2], by:

$$R^s = \left|r^s\right|^2 \text{ and } R^p = \left|r^p\right|^2 . \tag{4}$$

For normal incidence, $\theta_i = 0$, the polarization dependence disappears and Eq. 3 reduces to the well-known expression for bulk surface reflectivity (Born & Wolf, 1999):

$$R = \left|\frac{\hat{n}-1}{\hat{n}+1}\right|^2 = \frac{(n-1)^2 + k^2}{(n+1)^2 + k^2} . \tag{5}$$

In any absorbing material (i.e., with $k > 0$) the light transmitted through the medium is attenuated in accordance with the Beer-Lambert law:

$$I(z) = I_o \, exp(-\alpha z) \tag{6}$$

where I_o is the intensity of light entering the surface, $\alpha = 4\pi k/\lambda$ is the linear attenuation coefficient of the medium at the wavelength λ, and z is the spatial coordinate with its origin at the surface. The inverse of the attenuation coefficient is known as the optical penetration depth

$$d_{opt} = \alpha^{-1} = \lambda / 4\pi k , \tag{7}$$

and it is the distance over which the light intensity is attenuated by $1/e$.

While the development above for the Fresnel coefficients assumes a semi-infinite medium (i.e., a single interface separating the two media), the significance of Eq. 6 is that any material whose of thickness $d >> d_{opt}$ can be considered optically thick, in the sense that it will behave the same as a semi-infinite medium. What constitutes an optically thick layer ultimately depends on the value of the complex part of the refractive index, k, as described in Eq. 7. For example, the penetration depth of silicon at $\lambda = 0.3$ μm is $d_{opt} \approx 5.8$ nm, very similar to that of aluminium at $\lambda = 0.4$ μm or gold at $\lambda = 0.7$ μm (Schulz, 1954); at longer wavelengths the penetration depth in silicon increases by over three orders of magnitude (on the order of several micrometers) due to the drastic decrease in the value of k. As we will show, the distinction between optically thick and optically thin films will have profound implications in the treatment of the optical thermal coupling that exists in laser heated MEMS.

2.2 Optically thin and multilayered systems

A different approach must be used in instances where the thickness of the irradiated film is comparable to the optical penetration depth. Such conditions are of significant relevance for surface micromachined polysilicon devices, which generally can have layers and gaps with thicknesses on the order of a few μm (Carter et al., 2005; MEMS Technologies Department,

[2] As a consequence of the two polarization conditions, there will be two independent values for reflectivity. For unpolarized irradiation, it is common practice to take the average of the two reflectivity values as the resultant reflectivity.

2008)—comparable to optical penetration depths at visible-to-near infrared wavelengths (Phinney & Serrano, 2007; Serrano & Phinney, 2009; Serrano et al., 2009). In theses cases, depicted in Fig. 3, light transmitted across the first interface will encounter a second interface and undergo reflection and refraction. The process of reflection and refraction at both interfaces can repeat itself numerous times, as shown in Fig. 3, and with each reflection, the wave can undergo a phase change of 180°. If the incident light is monochromatic, with sufficiently large coherence length (i.e., laser light), then the multiple reflections will interfere with each other constructively and destructively. This thin film interference will yield deviations from the values obtained with Eqs. 3 and 4 for the optical response of the irradiated surface.

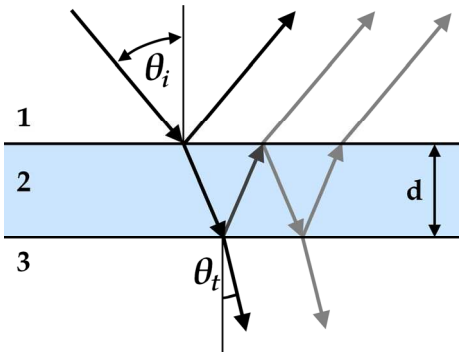

Fig. 3. Reflection and refraction in a multilayered system showing the multiple reflections from the two interfaces.

There are various ways to obtain a numerical description of the overall optical performance of such a multilayered system. The most common method is the transfer matrix method (Born & Wolf, 1999; Katsidis & Siapkas, 2002) whereby each individual layer is assigned a matrix of Fresnel coefficients, which capture the interaction of the incident wave with the layer. This method, while useful for obtaining the net response of the stratified structure, does not easily permit extracting information on how the energy is deposited within the layers, a detail of paramount importance when analyzing laser-irradiated MEMS. To obtain interlayer absorptance values, we turn to a similar analysis called the LTR method (Mazilu et al., 2001), which combines the layer responses in a modular form. This modularity then permits the extraction of the absorptances for the layers in the structure.

2.2.1 LTR method

The LTR method (Mazilu et al., 2001), which is stands for **L**eft-side reflectance, **T**ransmittance, and **R**ight-side reflectance, considers a stack of material irradiated from the left and right sides, as shown in Fig. 4. The technique leverages the fact that for an irradiated layered system only three terms are needed to fully describe its optical response—the reflectances of either side and a transmittance term. While most typically utilized for obtaining the net response of a stratified system, the modular nature of the LTR method facilitates the extraction of absorptance values for each individual layer, making it particularly useful for laser-irradiated MEMS (Serrano & Phinney, 2009; Serrano et al., 2009).

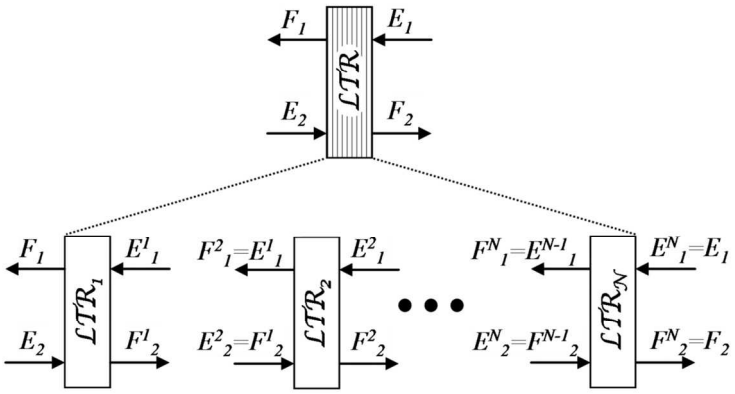

Fig. 5. Schematic representation of the LTR method. A multilayer stack is represented by an LTR element, where each layer is also made up of an LTR element.

This technique is similar to the transfer matrix method in that each layer is assigned a mathematical entity made up of the reflection and transmission coefficients for the layer. However, unlike the matrix method where the layer matrix depends on the properties of the media surrounding the layer, the coefficients are referenced with respect to vacuum (i.e., a wave is considered to be travelling into or from vacuum), simplifying the calculations and giving the technique its modularity. Thus, a three-element LTR vector containing the left- and right-side reflection coefficients, as well as the transmission coefficient, is defined as:

$$\mathbf{X} = \begin{pmatrix} L \\ T \\ R \end{pmatrix} = \begin{pmatrix} r\dfrac{1-p^2}{1-p^2r^2} \\ p\dfrac{1-r^2}{1-p^2r^2} \\ r\dfrac{1-p^2}{1-p^2r^2} \end{pmatrix}. \tag{8}$$

For a wave incident at an angle θ_i upon a layer of thickness d and refractive index $\hat{n}$, the coefficient p in Eq. 8 considers propagation in the medium and is defined as:

$$p = exp\left(i\tfrac{2\pi}{\lambda}d\sqrt{\hat{n}^2 - sin^2\theta_i}\right), \tag{9}$$

whereas the coefficient r considers reflection from the interfaces and for the two possible polarization conditions[3] is given by Eq. 3. The Fresnel coefficients above assume the wave

[3] As discussed in footnote 2, this method will yield polarization-dependent results for reflectance, transmittance, and absorptances. For unpolarized irradiation, the accepted value is the average of the two polarization cases.

travels from vacuum through the layer and out into vacuum once again. If the amplitudes of the fields incident on the layer from the right and the left are given, as shown in Fig. 5, by E_1 and E_2, respectively, the elements of $\mathbf{X}$ can be used to describe the amplitudes of the fields, F_1 and F_2, exiting the layer as:

$$F_1 = TE_1 + LE_2, \text{ and} \tag{10}$$

$$F_2 = RE_1 + TE_2. \tag{11}$$

The LTR method additionally defines a vector for a single interface: one for an interface with a wave travelling from vacuum into a medium of index $\hat{n}$ ($\mathbf{S}_{01}$) and another for a wave travelling from the medium into vacuum ($\mathbf{S}_{10}$):

$$\mathbf{S}_{01}(\hat{n}) = \begin{pmatrix} L \\ T \\ R \end{pmatrix} = \begin{pmatrix} r \\ t_{01} \\ -r \end{pmatrix}, \text{ and} \tag{12}$$

$$\mathbf{S}_{10}(\hat{n}) = \begin{pmatrix} L \\ T \\ R \end{pmatrix} = \begin{pmatrix} -r \\ t_{10} \\ r \end{pmatrix}, \tag{13}$$

where the coefficient r is given in Eq. 3 for the two polarization conditions, and

$$t_{01}^{s} = \frac{2\cos\theta_i}{\cos\theta_i + \sqrt{\hat{n}^2 - \sin^2\theta_i}}, \quad t_{01}^{p} = \frac{2\hat{n}\cos\theta_i}{\hat{n}^2\cos\theta_i + \sqrt{\hat{n}^2 - \sin^2\theta_i}}, \tag{14}$$

$$t_{10}^{s} = \frac{2\hat{n}\cos\theta_i}{\cos\theta_i + \sqrt{\hat{n}^2 - \sin^2\theta_i}}, \text{ and } t_{10}^{p} = \frac{2\hat{n}^2\cos\theta_i}{\hat{n}\cos\theta_i + \sqrt{\hat{n}^2 - \sin^2\theta_i}}. \tag{15}$$

Combination of multiple layers is implemented by the use of a composition rule, as shown below for two layers. Under the LTR scheme, each layer is considered a separate entity, separated from adjacent layers by a zero- thickness vacuum layer, such that the wave exits one layer into vacuum and enters the next layer from vacuum.

$$\mathbf{LTR} = \mathbf{X}_1 \oplus \mathbf{X}_2 = \begin{pmatrix} L_1 \\ T_1 \\ R_1 \end{pmatrix} \oplus \begin{pmatrix} L_2 \\ T_2 \\ R_2 \end{pmatrix} = \begin{pmatrix} L_1 + \dfrac{L_2 T_1^2}{1 - R_1 L_2} \\ \dfrac{T_1 T_2}{1 - R_1 L_2} \\ R_2 + \dfrac{R_1 T_2^2}{1 - R_1 L_2} \end{pmatrix} = \begin{pmatrix} \mathcal{L} \\ \mathcal{T} \\ \mathcal{R} \end{pmatrix}. \tag{16}$$

This rule enables modeling of a multilayer structure by sequential application of the composition rule to all the layers in the stack including the media on the left and right side of the multilayer structure.

$$\mathbf{LTR} = \mathbf{S}_{10}(\hat{n}_L) \oplus \mathbf{X}_1 \oplus \mathbf{X}_2 \oplus \cdots \oplus \mathbf{X}_{N-1} \oplus \mathbf{X}_N \oplus \mathbf{S}_{01}(\hat{n}_R) = \begin{pmatrix} \mathcal{L} \\ \mathcal{T} \\ \mathcal{R} \end{pmatrix} \tag{17}$$

Since the result of the composition is another LTR vector, if the fields E_1 and E_2 incident on the stack are known, then the remaining fields, F_1 and F_2, can be easily found using Eqs. 10 and 11.

While the LTR construct is useful for capturing the response of a multilayered structure irradiated from the front and the back (left and right in Fig. 3), only front-side illumination is considered here, as that is the most common configuration encountered in MEMS applications. For single-sided illumination the structure is assumed to be illuminated only from the left (i.e., $E_1 = 0$ in Fig. 5), and

$$\mathcal{L} = F_1/E_2 \text{ (left side reflection);} \tag{18}$$

$$\mathcal{T} = F_2/E_2 \text{ (transmission);} \tag{19}$$

$$\mathcal{R} = 0 \text{ (right side reflection).} \tag{20}$$

The total reflected, transmitted, and absorbed intensities are then:

$$R = |\mathcal{L}|^2, \tag{21}$$

$$T = |\mathcal{T}|^2 \frac{Re(n_R \cos\theta_R)}{Re(n_L \cos\theta_L)}, \text{ and} \tag{22}$$

$$A = 1 - R - T. \tag{23}$$

If the incident medium on the left is vacuum or air, Eq. 22 can be rewritten fully in terms of the angle of incidence and the substrate index, $\hat{n}_{sub}$, as

$$T = |\mathcal{T}|^2 \frac{Re\left(\sqrt{\hat{n}_{sub}^2 - sin^2\theta_i}\right)}{\cos\theta_i}. \tag{24}$$

With the fields on the left- and right-most layers defined, the fields entering and exiting each layer can be obtained by recursively applying Eqs. 10 and 11 to each layer. Once these fields are defined, the individual layer absorptances can be easily obtained by noting that each layer is referenced to vacuum and the absorptance is simply the difference between the entering and exiting field magnitudes:

$$A_i = |E_1^i|^2 + |E_2^i|^2 - |F_1^i|^2 - |F_2^i|^2, \tag{25}$$

where the left-most fields of the first layer and the right-most fields for the last layer are obtained from Eqs. 18 and 19.

2.2.2 MEMS

As discussed in the previous section, the optical response of laser-irradiated materials depends strongly on various parameters. For optically thick materials, the refractive index of the irradiated medium determines the reflectivity of the surface and thus the fraction of the energy that is deposited in the material. When the optical penetration depth is comparable to film thickness, the geometry and composition of the structure becomes as important as refractive index in dictating the optical response. This becomes evident when analyzing the response of sacrificial micromachined MEMS fabricated from polysilicon.

In polysilicon-based MEMS the typical layer thickness is approximately 2 μm, with intermediate gaps of the same order (Carter et al., 2005; MEMS Technologies Department 2008). Such thicknesses are comparable to the penetration depth for both silicon and polysilicon for wavelengths above 550 nm (Jellison Jr & Modine, 1982a, 1982b; Lubberts et al., 1981; Xu & Grigoropoulos, 1993) and therefore the likelihood for thin film interference, as explained above, increases. Indeed, calculations carried out for air-spaced polysilicon structure fabricated from Sandia National Laboratories' SUMMiT-V™ process (MEMS Technologies Department, 2008), as shown in Fig. 6, show that the absorptance of the top-most layer can vary significantly as a function of the layer thickness. The multiple reflections from the various layers in the structure lead to conditions of local maxima and minima for different layer thicknesses. These extrema correspond to thicknesses where the interference between the multiply reflected waves is fully constructive or destructive as will be shown later.

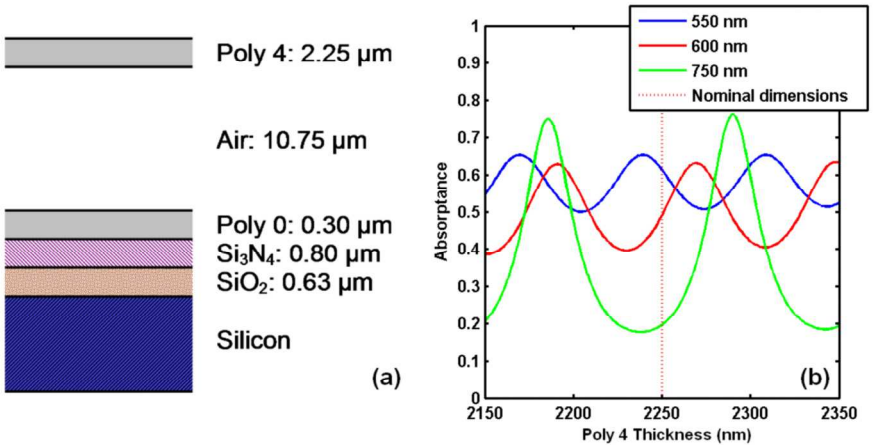

Fig. 6. (a) Schematic of a SUMMiT V™ polysilicon MEMS structure and (b) its optical response at different wavelengths as a function of the thickness of the top-most layer.

The variation in the amplitude and width of the absorptance peaks in this structure is related to the relative reflectivity of the two polysilicon surfaces at the particular wavelength much like a Fabry-Perot cavity (Born & Wolf, 1999) and will ultimately depend on the overall composition of the multilayered structure. For a coupled optical-thermal analysis, the existence of these periodic variations in the absorptance must be taken into account to predict the thermal behavior of laser-irradiated MEMS accurately.

3. Optical-thermal coupling in laser-irradiated MEMS

The previous section detailed the response of MEMS optical systems in strictly athermal terms. However, in laser-irradiated MEMS or MEMS exposed to extreme thermal environments the consequences of a changing thermal environment could be significant, especially in regards to the optical response. For simplicity, we shall consider cases where the incident laser energy is responsible for any temperature fluctuation in the irradiated structure, although the same principles are valid for structures subject to bulk external heating and laser irradiation (Burns & Bright, 1998).

Laser irradiation of an absorbing structure, such as micromachined polysilicon MEMS, will lead to a corresponding temperature increase. The magnitude of the induced temperature rise will depend on several factors, including the geometry, and thermal and optical properties of the irradiated materials. Because all of the parameters that play a role in determining the energy deposition exhibit some temperature dependence, the laser-induced heating of the structure will be dynamic in nature as the properties change during the heating event.

3.1 Temperature-induced geometry changes

We have already seen the potential effects of different layer thicknesses on the absorptance of an irradiated structure. However, while those fluctuations might arise out of manufacturing variability, the same effect can be observed during the heating of an as-built device. Geometrical and dimensional considerations during the heating result from any temperature-induced displacement and deformation of the MEMS when exposed to elevated temperatures (Knoernschild et al., 2010; Phinney et al., 2006). If the irradiating wavelength is in the optically thick regime for the irradiated material, the dimensional changes do not have a significant effect in the optical response of the structure since the incident energy is fully absorbed within the material. Nevertheless, depending on the structure, small deflections and deformations could have a significant effect on the heat transfer mechanisms on the heated device (Gallis et al., 2007; Wong & Graham, 2003).

When the conditions are such that thin film interference becomes important in the optical response, particularly for multilayered systems, the deformation will have a more dramatic effect. Depending on the design and geometry of the irradiated structure, the heating can alter both the thickness of the individual layers (via thermal expansion) and the spacing between them (via thermal expansion, buckling, etc.). Such deformations will produce changes in the absorptance of the laser irradiation, as shown in Fig. 7 for a Poly4 SUMMiT V™ structure similar to the one described by Phinney et al, (Phinney et al., 2006) and shown in Fig. 6a. The cantilevered structure in that reference suffered deflections of over 10 μm during laser irradiation. In Fig. 7, just a variation in the air gap height of ±500 nm suffices to demonstrate the type of deflection-induced changes in absorptance encountered in these tests. Assuming the deflection is caused by the temperature excursion of the structure, then a small change in gap height can lead to as much as a six-fold change in absorptance.

Additionally, due to the phase changes upon reflection, the trends in absorptance repeat for different values of thicknesses and gaps, as seen in Figs 6 and 7. The recurrence period can be estimated from Eq. 9 by finding the thickness increase Δd for which the path length difference is equivalent to an integer multiple of π:

$$\Delta d = \frac{m\lambda}{2\,Re\left(\sqrt{\hat{n}^2 - sin^2\,\theta_i}\right)},\ m = 1, 2, 3\ldots \tag{26}$$

which, for the 800 nm example discussed, yields a recurrence period of 400 nm.

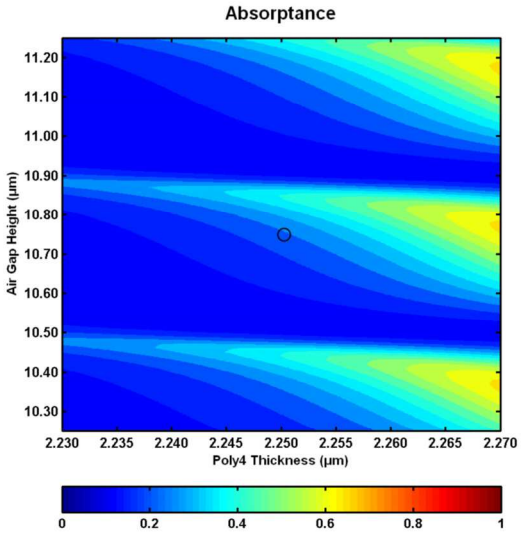

Fig. 7. Absorptance map for the geometry shown in Fig. 6a for λ = 808 nm as a function of layer and gap dimensions. The circle indicates the nominal dimensions for the geometry.

The outcome of such a variation in energy deposition can be detrimental—an increase in absorptance will cause additional heating and possibly lead to damage—or beneficial—a decrease in absorptance will permit the structure to withstand higher incident powers and avoid damage (Serrano & Phinney, 2009). Which situation is encountered with a particular device will depend on the irradiating conditions (wavelength and incidence angle), the optical properties, as well as the initial condition and the geometry of the device and the thermomechanical response of the structure. Because MEMS are primarily mechanical devices, these thermomechanical effects can typically be accounted and corrected for to reduce their contribution, much like it is done for electrically heated devices (Sassen et al., 2008).

3.2 Temperature-induced optical changes

In addition to purely mechanical effects caused by the heating, the temperature excursion will induce changes in the optical and thermal properties of the irradiated materials. While the variations in the thermal properties with temperature play a very important role in the thermal behavior of any laser-irradiated structure, their effects are generally noticeable for large temperature excursions. As we will show, the role of the temperature dependence of the material optical properties is, in some cases, more dominant and leads to marked changes in the thermal and optical performance of the irradiated structure over small temperature excursions.

For silicon-based materials, the complex index of refraction has been extensively studied as a function of temperature (Jellison Jr & Modine, 1982a, 1983; Sun et al., 1997; Xu & Grigoropoulos, 1993; Yavas et al., 1993). These works all show that the real part of the refractive index depends linearly with temperature:

$$n = n_o + \frac{dn}{dT}\left(T - T_o\right) \tag{27}$$

where n_o is the index at a reference temperature T_o and the slope $\frac{dn}{dT}$ typically has values on the order of 10^{-4} K^{-1} (Jellison Jr & Modine, 1982a, 1983; Sun et al., 1997; Xu & Grigoropoulos, 1993). The complex portion of the index, on the other hand, follows an exponential trend of the form:

$$k = k_o e^{\left(\frac{T - T_o}{T_R}\right)} \tag{28}$$

where k_o is complex index at T_o and the temperature T_R is an empirically determined reference temperature, which ranges in value from 498 K for bulk silicon (Jellison Jr & Modine, 1982a, 1983) to 680 K for different types of polysilicon (Sun et al., 1997; Xu & Grigoropoulos, 1993).

In optically thick systems, the change in complex refractive index will manifest itself as a change in surface reflectivity as a function of temperature. For silicon and polysilicon, this change is on the order of 10^{-5} K^{-1} (Jellison Jr & Modine, 1983) such that its impact on the thermal and mechanical response of irradiated devices is small. The same cannot be said for multilayered structures that are optically thin. In this case, the linear increase in the real part of the refractive index increases the effective path length difference between multiply reflected waves, changing the conditions for constructive and destructive interference from those present at the initial temperature. The exponential increase in the complex portion of the index, however, leads to a decrease in the optical penetration depth, reducing the effect of interference from deeper layers in the material. More importantly, the interplay between the two trends, when applied to the thin film interference equations discussed in the previous section, leads to temperature-dependent variations in the absorptance, as shown in Fig. 8 for the structure in Fig. 6a irradiated with 800 nm light. The most noticeable characteristic of the curves is the presence of temperature-periodic peaks. These result from the increase in the path length difference as the real portion of the index increases with temperature as given by Eq. 27. When the condition for fully destructive interference of the surface reflected waves is met, the absorptance of the layer increases. This condition is satisfied for

$$\tfrac{2\pi}{\lambda} d\, Re\left(\sqrt{\left(\hat{n} + \Delta\hat{n}\right)^2 - sin^2\,\theta_i}\right) = \tfrac{2\pi}{\lambda} d\, Re\left(\sqrt{\hat{n}^2 - sin^2\,\theta_i}\right) + m\pi \text{ , } (m = 1, 2, 3, \ldots). \tag{29}$$

Solving the above relation for $\Delta\hat{n}$, and relating that to the temperature change through Eq. 27, we get:

$$\Delta T = Re\left(\frac{m\lambda\hat{n}}{2z\sqrt{\hat{n}^2 - sin^2\,\hat{\theta}_i}}\right)\left(\frac{dn}{dT}\right)^{-1}. \tag{30}$$

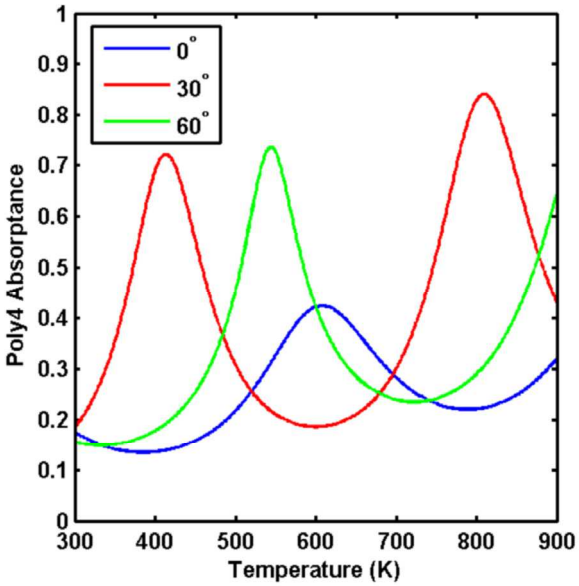

Fig. 8. Absorptance as a function of temperature and incidence angle for the geometry shown in Fig. 6a for λ = 800 nm.

The consequences of the peaks and valleys are significant for the behavior of laser-irradiated polysilicon MEMS. An incident laser on the surface will induce heating, leading to a change in absorptance, and corresponding changes in the sample temperature. The non-linear absorptance response thus creates stable and unstable conditions depending on the temperature of the sample. For temperatures in the range where the slope of the absorptance curves is negative, the system can achieve equilibrium since a temperature rise leads to decreased absorptance, reducing the energy deposition. For temperatures lying in the opposite side of the absorptance peak, the increase in temperature induces an increase in absorptance, leading to a significant increase in energy deposition and consequently an even greater temperature rise.

4. Laser-induced damage of polycrystalline silicon MEMS

The combination of multilayered design, coupled with temperature-induced changes in the optical properties ultimately leads to failure of laser-irradiated MEMS. From a design perspective, in addition to considering the primary mechanical function of the device—such as an actuator (Baglio et al., 2002; Oliver et al., 2003; Phinney et al., 2005; Phinney & Serrano, 2007; Serrano et al., 2005) or a shutter (Wong & Graham, 2003)—the design should also consider the optical and thermal behavior of the structure to reduce the likelihood of damage. To gain a better understanding of the design concerns associated with polysilicon optical MEMS, various experiments have been carried out that have provided insights into the importance of composition, optical energy deposition and thermal transport of heating (Baglio et al., 2002; Oliver et al., 2003; Phinney & Serrano, 2005; Serrano & Phinney, 2009;

Serrano et al., 2009). In this section, we will briefly look over some of the experimental results for laser-induced damage in the context of the optical and thermal analysis discussed in the previous sections.

For optically-powered MEMS thermal actuators (Baglio et al, 2002; Phinney & Serrano, 2007; Serrano & Phinney, 2009) most of the studies have mainly focused on empirically establishing the threshold power for damage. Typically, damage is defined as visible damage at the surface—in the form of a crater-like feature as shown Fig. 9—after initial irradiation of the surface. However, these studies also showed that damage could be initiated after prolonged exposure (on the order of minutes) to the laser irradiation, indicating the presence of a slow heating process. This behavior agrees qualitatively with the concepts discussed in the previous section. Thermal equilibrium for the irradiated structure cannot be achieved for the temperature where the absorptance exhibits a peak. Therefore, the system reaches a metastable equilibrium in the valleys of the absorptance curve as shown in Figs. 6 and 8. These valleys, however, do not represent a flat absorptance, but rather a slowly varying one. Thus, as the devices slowly heats up, the material's absorptance increases until the next absorptance peak is encountered and the deposited energy density is enough to cause damage of the device. The time-delayed damage observed is then evidence of the slow heating and approach of the temperature to the absorptance peak.

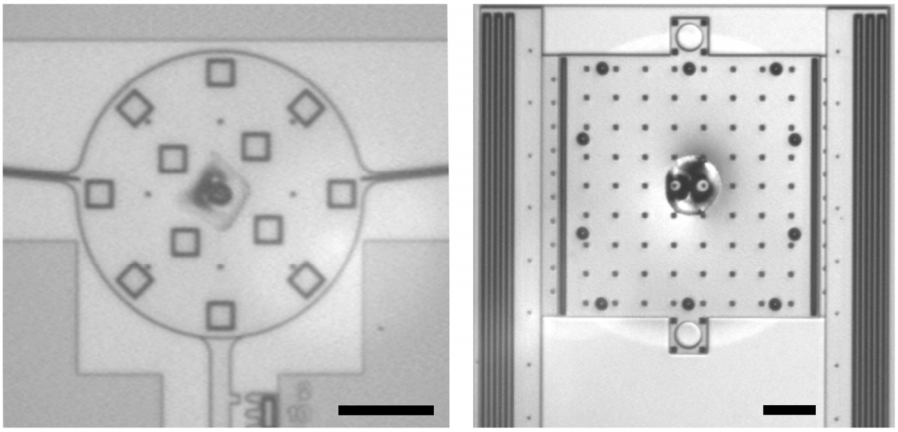

Fig. 9. Typical laser-induced damage on polysilicon MEMS structures. The scale bar on both is equivalent to 50 μm. (Phinney & Serrano, 2007; Serrano & Phinney, 2009)

The effect of the absorptance peaks can also explain the damage thresholds in laser-irradiated microsystems (Serrano & Phinney, 2009) that do not correlate with the number of layers present in the structure. The results show that a single-layer structure exhibited greater power handling capability than various multilayered ones. In said structures, the thin film interference phenomena leads to a minimum in absorptance, like the one shown Fig. 8 for normal incidence near room temperature. This minimum, coupled to improved

heat dissipation to the underlying substrate, permits the single layer structure to exhibit increased robustness to the laser irradiation compared to the multilayered structures.
The optical-thermal effects can also explain the temperature discontinuities observed in the temperature measurements of laser irradiated cantilevers and actuators (Serrano & Phinney, 2007; Serrano et al., 2009), shown in Fig. 9. As predicted above, the discontinuity corresponds to the presence of the peak in the absorptance curve. The surface temperature increases rapidly by 200 K as the peak is encountered. The temperature-power relationship regains a linear relation after the temperature reaches the opposite side of the absorptance peak. Numerical simulations of this experiment, utilizing the non-linear absorptance and known material and geometrical parameters for the irradiated structure, are in good agreement with the measured values, reproducing temperature discontinuity. This type of sudden increase in the temperature makes predicting a threshold power for laser damage in polysilicon structures extremely challenging without accurate knowledge of optical and dimensional properties.

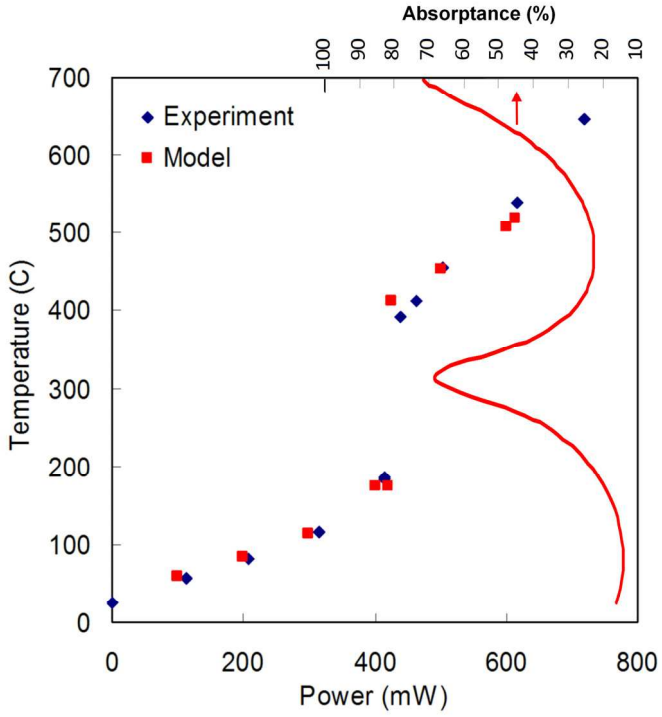

Fig. 10. Measured and modeled temperatures of a polysilicon MEMS structure measured irradiated with an λ = 808 nm laser. The discontinuity in the temperature results from a peak in the absorptance of the irradiated layer due to thin film interference effects (Serrano et al., 2009).

5. Conclusion

Understanding the thermal and optical response of laser-irradiated microsystems requires careful consideration of not only the individual thermal, optical, and mechanical parameters, but also the coupling that exists between them. Of particular importance is the impact that the change in the optical properties with temperature can have in the performance and reliability of these structures. To gain insight into the role that temperature and geometry play in the optical performance of these devices, one must utilize the basic optical relations in a way that is compatible with thermal analyses of a laser-heated structure. The LTR method has proven to be a very useful technique in these types of analyses since it can easily incorporate temperature dependant optical properties and readily provide the interlayer absorptances for the irradiated structures.

Once the temperature and optical fields are coupled in the analysis, a more accurate picture emerges of the thermal and optical behavior of the irradiated device. These coupled optical-thermal effects give rise to non-linear absorptance that can, in some instances, lead to increased resistance to laser damage by dynamically reducing the absorptance as the incident laser power is increased, while in other cases, the non-linear effects compound to enhance absorptance of the incident laser energy producing rapid temperature increases that eventually lead to device damage. A quantitative estimation of device robustness to determine in which regime of damage susceptibility a particular structure resides in therefore requires a complete description of the overall irradiating conditions as well as the device composition. For polysilicon-based devices, this type of analysis has shown reasonable agreement with the experimentally-observed thermal behavior, and can explain the observed damage trends of the laser-irradiated structures.

6. Acknowledgment

The authors would like to acknowledge the help and assistance of Allen Gorby, James Rogers, Wayne Trott, and Jaime Castaneda. Sandia National Laboratories is a multi-program laboratory managed and operated by Sandia Corporation, a wholly owned subsidiary of Lockheed Martin Corporation, for the U.S. Department of Energy's National Nuclear Security Administration under contract DE-AC04-94AL85000.

7. References

Andrews, J. R., Martinez, T., Teare, S. W., Restaino, S. R., Wilcox, C. C., Santiago, F. & Payne, D. M. (2011). A multi-conjugate adaptive optics testbed using two MEMS deformable mirrors. *Proceedings of MEMS Adaptive Optics V,* San Francisco, CA, USA

Andrews, J. R., Teare, S. W., Restaino, S. R., Martinez, T., Wilcox, C. C., Wick, D. V., Cowan, W. D., Spahn, O. B. & Bagwell, B. E. (2008). Performance of a MEMS reflective wavefront sensor. *Proceedings of SPIE,* Vol. 6888, pp. 68880C

Baglio, S., Castorina, S., Fortuna, L. & Savalli, N. (2002). Novel microactuators based on a photo-thermo-mechanical actuation strategy. *Proceedings of IEEE Sensors*, Orlando, FL, USA

Baker, M. S., Plass, R. A., Headley, T. J. & Walraven, J. A., (2004), *Final Report: Compliant Thermo-Mechanical MEMS Actuators LDRD #52553*, SAND2004-6635, Sandia National Laboratories, Albuquerque, New Mexico

Born, M. & Wolf, E. (1999). Principles of Optics: Electromagnetic Theory of Propagation, Interference and Diffraction of Light (7th edition), Cambridge University Press, Cambridge

Burns, D. M. & Bright, V. M. (1998). Optical power induced damage to microelectromechanical mirrors. *Sensors and Actuators A,* Vol. 70, No. 1-2, pp. 6-14

Carter, J., Cowen, A., Hardy, B., Mahadevan, R., Stonefield, M. & Wilcenski, S., (2005), *PolyMUMPs Design Handbook, Revision 11.0,* MEMSCAP, Inc.

Gallis, M. A., Torczynski, J. R. & Rader, D. J. (2007). A computational investigation of noncontinuum gas-phase heat transfer between a heated microbeam and the adjacent ambient substrate. *Sensors and Actuators A: Physical,* Vol. 134, No. 1, pp. 57-68

Jellison Jr, G. E. & Modine, F. A. (1982a). Optical absorption of silicon between 1.6 and 4.7 eV at elevated temperatures. *Applied Physics Letters,* Vol. 41, No. 2, pp. 180-182

Jellison Jr, G. E. & Modine, F. A. (1982b). Optical constants for silicon at 300 and 10 K determined from 1.64 to 4.73 eV by ellipsometry. *Journal of Applied Physics,* Vol. 53, No. 5, pp. 3745-3753

Jellison Jr, G. E. & Modine, F. A. (1983). Optical functions of silicon between 1.7 and 4.7 eV at elevated temperatures. *Physical Review B,* Vol. 27, No. 12, pp. 7466-7472

Katsidis, C. C. & Siapkas, D. I. (2002). General Transfer-Matrix Method for Optical Multilayer Systems with Coherent, Partially Coherent, and Incoherent Interference. *Applied Optics,* Vol. 41, No. 19, pp. 3978-3987

Knoernschild, C., Changsoon, K., Gregory, C. W., Lu, F. P. & Jungsang, K. (2010). Investigation of Optical Power Tolerance for MEMS Mirrors. *Journal of Microelectromechanical Systems,* Vol. 19, No. 3, pp. 640-646

Knoernschild, C., Kim, C., Lu, F. P. & Kim, J. (2009). Multiplexed broadband beam steering system utilizing high speed MEMS mirrors. *Optics Express,* Vol. 17, No. 9, pp. 7233-7244

Lubberts, G., Burkey, B. C., Moser, F. & Trabka, E. A. (1981). Optical properties of phosphorus-doped polycrystalline silicon layers. *Journal of Applied Physics,* Vol. 52, No. 11, pp. 6870-6878

Mazilu, M., Miller, A. & Donchev, V. T. (2001). Modular Method for Calculation of Transmission and Reflection in Multilayered Structures. *Applied Optics,* Vol. 40, No. 36, pp. 6670-6676

MEMS Technologies Department, (2008), *SUMMiT V™ Five Level Surface Micromachining Technology Design Manual: Version 3.1a*, Sandia Report No. SAND2008-0659P, Sandia National Laboratories, Albuquerque, NM

Oliver, A. D., Vigil, S. R. & Gianchandani, Y. B. (2003). Photothermal surface-micromachined actuators. *IEEE Transactions on Electron Devices,* Vol. 50, No. 4, pp. 1156-1157

Phinney, L. M., Klody, K. A., Sackos, J. T. & Walraven, J. A., (2005). Damage of MEMS thermal actuators heated by laser irradiation. *Proceedings of SPIE,* Vol. 5716, pp. 81-88

Phinney, L. M. & Serrano, J. R. (2007). Influence of target design on the damage threshold for optically powered MEMS thermal actuators. *Sensors and Actuators A,* Vol. 134, No. 2, pp. 538-543

Phinney, L. M., Spahn, O. B. & Wong, C. C. (2006). Experimental and computational study on laser heating of surface micromachined cantilevers. *Proceedings of SPIE,* Vol. 6111, pp. 611108

Plass, R. A., Baker, M. S. & Walraven, J. A. (2004). Electrothermal actuator reliability studies. *Proceedings of SPIE,* Vol. 5343, pp. 15-21

Sassen, W. P., Henneken, V. A., Tichem, M. & Sarro, P. M. (2008). Contoured thermal V-beam actuator with improved temperature uniformity. *Sensors and Actuators A: Physical,* Vol. 144, No. 2, pp. 341-347

Schulz, L. G. (1954). The Optical Constants of Silver, Gold, Copper, and Aluminum. I. The Absorption Coefficient k. *Journal of the Optical Society of America,* Vol. 44, No. 5, pp. 357-362

Serrano, J. R. & Phinney, L. M. (2008). Displacement and Thermal Performance of Laser-Heated Asymmetric MEMS Actuators. *Journal of Microelectromechanical Systems,* Vol. 17, No. 1, pp. 166-174

Serrano, J. R. & Phinney, L. M. (2009). Effects of layers and vias on continuous-wave laser heating and damage of surface-micromachined structures. *Journal of Micro/Nanolithography, MEMS and MOEMS,* Vol. 8, No. 4, pp. 043030

Serrano, J. R. & Phinney, L. M. (2007). Micro-Raman thermometry of laser heated surfaces. *Proceedings of ASME InterPACK 2007,* Vancouver, BC, Canada

Serrano, J. R., Phinney, L. M. & Brooks, C. F. (2005). Laser-Induced damage of polycrystalline silicon optically powered MEMS actuators. *Proceedings of ASME InterPACK 2005,* San Franscisco, CA, USA

Serrano, J. R., Phinney, L. M. & Rogers, J. W. (2009). Temperature amplification during laser heating of polycrystalline silicon microcantilevers due to temperature-dependent optical properties. *International Journal of Heat and Mass Transfer,* Vol. 52, No. 9-10, pp. 2255-2264

Sun, B. K., Zhang, X. & Grigoropoulos, C. P. (1997). Spectral optical functions of silicon in the range of 1.13-4.96 eV at elevated temperatures. *International Journal of Heat and Mass Transfer,* Vol. 40, No. 7, pp. 1591-1600

Wong, C. N. C. & Graham, S. (2003). Investigating the thermal response of a micro-optical shutter. *IEEE Transactions on Components and Packaging Technologies,* Vol. 26, No. 2, pp. 324-331

Xu, X. & Grigoropoulos, C. P. (1993). High temperature radiative properties of thin polysilicon films at the $\lambda = 0.6328$ μm wavelength. *International Journal of Heat and Mass Transfer,* Vol. 36, No. 17, pp. 4163-4172

Yavas, O., Do, N., Tam, A. C., Leung, P. T., Leung, W. P., Park, H. K., Grigoropoulos, C. P., Boneberg, J. & Leiderer, P. (1993). Temperature dependence of optical properties for amorphous silicon at wavelengths of 632.8 and 752 nm. *Optics Letters,* Vol. 18, No. 7, pp. 540-542

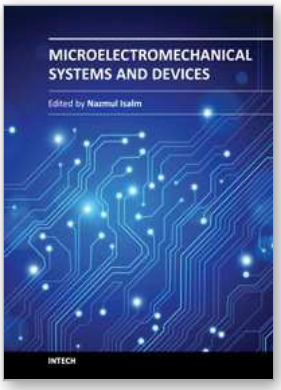

Microelectromechanical Systems and Devices

Edited by Dr Nazmul Islam

ISBN 978-953-51-0306-6
Hard cover, 480 pages
Publisher InTech
Published online 28, March, 2012
Published in print edition March, 2012

The advances of microelectromechanical systems (MEMS) and devices have been instrumental in the demonstration of new devices and applications, and even in the creation of new fields of research and development: bioMEMS, actuators, microfluidic devices, RF and optical MEMS. Experience indicates a need for MEMS book covering these materials as well as the most important process steps in bulk micro-machining and modeling. We are very pleased to present this book that contains 18 chapters, written by the experts in the field of MEMS. These chapters are groups into four broad sections of BioMEMS Devices, MEMS characterization and micromachining, RF and Optical MEMS, and MEMS based Actuators. The book starts with the emerging field of bioMEMS, including MEMS coil for retinal prostheses, DNA extraction by micro/bio-fluidics devices and acoustic biosensors. MEMS characterization, micromachining, macromodels, RF and Optical MEMS switches are discussed in next sections. The book concludes with the emphasis on MEMS based actuators.

INTECH
open science | open minds

InTech Europe
University Campus STeP Ri
Slavka Krautzeka 83/A
51000 Rijeka, Croatia
Phone: +385 (51) 770 447
Fax: +385 (51) 686 166
www.intechopen.com

InTech China
Unit 405, Office Block, Hotel Equatorial Shanghai
No.65, Yan An Road (West), Shanghai, 200040, China
中国上海市延安西路65号上海国际贵都大饭店办公楼405单元
Phone: +86-21-62489820
Fax: +86-21-62489821